J. Fluid Mech. (2001), *vol.* 428, *pp.* 171–183. Printed in the United Kingdom

Contact line instability in spontaneous spreading of a drop on a solid surface

By P. NEOGI

Chemical Engineering Department, University of Missouri-Rolla, Rolla, MO 65409-1230, USA

(Received 26 July 1999 and in revised form 9 August 2000)

The wetting kinetics of a drop on a solid surface is measured by observing the movement of the contact line, which is often seen to be unstable, showing a scalloped profile. Many factors have been cited, which, although they can cause instability, can also be eliminated from the experiments, but still the instabilities appear. The basic shape of a spreading drop has a large curvature localized in the vicinity of the contact line as determined by microscopy. It is shown here using linear stability analysis that this curvature can destabilize the contact line region. When the drop profile is disturbed from a basic thickness of $\bar{h}$ to $\bar{h} + h'$, there are two contributions from h' in the form of added Laplace pressure. One of these is commonly accounted for in the stability analyses. The other is not, and occurs only if the basic shape has a curvature, and the drop has a large curvature near the apparent dynamic contact line, but only for a wetting liquid. This is why instability is not reported in the case of spreading of drops of non-wetting liquids. It also explains why instability gives rise to the changed spreading kinetics of drops that are sometimes reported in the literature, and suggests that as larger curvatures are expected in forced spreading those cases are probably accompanied quite frequently by unstable contact lines.

1. Introduction

The rate at which a drop spreads on a solid surface, which is called wetting or spreading kinetics, is often measured as a function of time. These measurements are taken by noting the position of the contact line, the line common to the liquid, solid and the ambient fluid. The study of wetting kinetics is important in coating processes (Kistler 1993) and shows that steady movement often breaks down at the contact line. In the case of spreading drops, the contact line instability is observed under the microscope in the form of a scalloped line or a line with periodic waves. The various cases observed are listed below, but first some preliminary comments on the experimental observations made on a spreading drop are noted.

Drop volumes used in experiments are 2–15 μl and at these values gravity does not play a role in spreading. The wetting velocities for spontaneous spreading are small, such that neither entrainment of the displaced fluid, nor the disappearance of the contact line, occur. The spreading drops of wetting liquids show under microscopy values of dynamic contact angles λ_a greatly different from the equilibrium value of zero. More accurate methods show that there is a thin precursor film ahead of the contact line, too thin to be seen under a microscope and which does subtend a zero contact angle on the solid substrate, in keeping with the fact that the liquid is wetting. The basic drop shapes under dynamic conditions show a segment of spherical profile, and λ_a is the angle obtained when this shape is extrapolated to the solid surface. The

basal radius is given by

$$\frac{r_0}{V^{1/3}} = a(c + t/V^{1/3})^{1/10}, \tag{1.1}$$

where a and c are constants, and c contains the initial conditions. V is the drop volume and t is the time. Equation (1.1) holds even when the ambient fluid is a viscous liquid, as long as the liquid is wetting. For a spherical cap profile and small dynamic contact angles $\lambda_a \approx 4V/\pi r_0^3$. Combining this with (1.1) one obtains what Kistler (1993) calls the Hoffman–Voinov–Tanner rule $\mathrm{d}r_0/\mathrm{d}t \propto \lambda_a^3$. Equation (1.1) is obtained under the lubrication theory approximation where drops are flat and move slowly. A problem arises in that the stresses at the contact line are seen to be infinite and a slip velocity is required at the solid–liquid interface to remove the singularity. The chief characteristic of the slip velocity is the slip length l which governs the magnitude of the slip and is hence expected to be small. The slip length is included in the term a in (1.1). Instability has been observed in the following cases.

(i) When a drop is spreading very rapidly, as in liquids of low viscosity, the contact line acquires a scalloped shape. Nieh, Ybarra & Neogi (1996) observed experimentally very rapid spreading and contact line instability for polymer solutions containing less than 5% polymer. But these effects disappeared at above 5% polymer, probably due to the lowered rates of spreading resulting from increased viscosities. At large velocities inertial forces should be important, and recently Lopez, Miksis & Bankoff (1997) have presented a linear stability analysis which shows that the inertial forces exert a destabilizing influence.

(ii) Fournier & Cazabat (1992) have shown experimentally that vaporization of an impurity from the leading edge can lead to contact line instability in that the contact line shows a periodic profile that is due to the Marangoni effect. Analysis of the Marangoni instability in a situation that bears some resemblance to a contact line has been given by Troian, Herzbolzheimer & Safran (1990). However, it is possible to make the liquid less volatile before use or saturate one liquid in another in a liquid–liquid system, such that no mass transfer and no Marangoni effect arise. Also, the liquid most commonly used in the experiments is polydimethyl siloxane which is generally free of volatile impurities since hydrocarbons and many organic liquids are insoluble in it. These systems also show a contact line instability.

(iii) In spite of experimental precautions Nieh *et al.* (1996) observed contact line instability at low spreading velocities, but only for wetting liquids. That is, they investigated the spreading kinetics of polystyrene in dibutyl phthalate over glass and found that only for one concentration and one molecular weight was the system wetting and only this case showed instability. They suggested that the nature of disjoining pressure in the thin film ahead of the drop could cause instability. In fact Ruckenstein & Jain (1974) have obtained theoretically a criterion for the kind of disjoining pressure which will lead to such an instability and which is indeed satisfied in polymer solutions (Ybarra, Neogi & MacElroy 1998). However, such thin films cannot be seen under a microscope and it is not known if instability at this level can propagate into the region of thick films which can be observed under a microscope and which show the contact line instability.

(iv) Joanny & Andelman (1987) have shown theoretically that when a drop spreads under a more viscous liquid, the contact line will become unstable. This is a form of viscous fingering which is well known in liquid–liquid systems (Miller 1978). Lin *et al.* (1998) have seen such instabilities in their experiments even when the two viscosities were about equal. In general, contact line instability for systems with no Marangoni

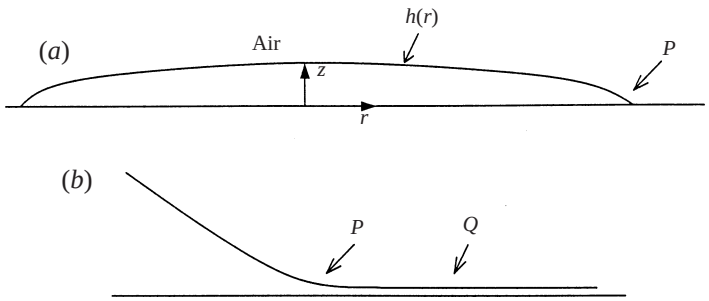

FIGURE 1. The shape of the drop and the region of interest are shown. The region P is where $r = \bar{r}_0$. Q is an enlarged view of the precursor, not visible under the magnification in (a).

effect and spreading at low rates is observed even under air in a few experiments (Nieh *et al.* 1996; Williams 1977; Léger *et al.* 1988).

Thus, instability is observed even when there is no mass transfer and hence no Marangoni effect, the spreading rates are slow such that the inertial forces can be neglected, and the ambient fluid is air such that there is no viscous fingering. The scallops have wavelengths which are quite small, barely seen with naked eye. Only Williams (1977) has reported quantitative values, which are 0.2 mm on a smooth surface. It arises more readily on rough solid surfaces (such as glass slides Nieh *et al.* 1996) than on smooth (such as vapour deposited surfaces Léger *et al.* 1988; Williams 1977), and more readily in liquid–liquid systems than in liquid under air. Instability has been observed only for wetting liquids.

The simplified model used here is that the spreading drop has a basic spherical cap shape, moves with the rate given in (1.1) and the basal radius (r_0) and the contact angle (λ_a) are the apparent ones as seen under a microscope. The precursor film is assumed to move faster than the drop (Lin, Ybarra & Neogi 1996) and is hence ignored. The existence of the precursor makes the curvature at the apparent contact line very large but localized, and very different from the value of the curvature of the drop as a whole. The drop is also assumed to have spread sufficiently such that it appears flat and the lubrication theory approximation applies. This geometry is shown schematically in figure 1. For such a model, linear stability analysis shown below predicts unstable contact lines with waves of small wavelengths. Two cases, one where the ambient fluid is inviscid and one where it is infinitely viscous, are considered. Fluids are taken to be Newtonian.

There are two features by which the present analysis is different from the existing studies. When the local drop thickness is perturbed from its base value of $\bar{h}$ to $\bar{h} + h'$, the perturbation adds a Laplace pressure proportional to $\nabla_s^2 h' + (4\bar{H}^2 - 2\bar{K})h'$. Here, ∇_s^2 is the Laplace–Beltrami operator and represents the term that is usually accounted for in the stability calculations (Bertozzi & Brenner 1997). $\bar{H}$ and $\bar{K}$ are the mean and Gaussian curvatures of the base profile $\bar{h}$. Thus, they are zeros when the base profile is a flat film. This term was derived by Tyupstov (1966) and Huh (1969). They, as well as Pitts (1974), used it to study the stability of static drops and Neogi & Adib (1985) to study the stability of rotating contact lines. It has a destabilizing effect and plays a crucial role here. The second feature is that to analyse the stability of the contact line region of a drop, it is necessary to allow the contact line to move. This requires one to use a slip velocity as explained earlier. Joanny & Andelman (1984) did not use slip and hence their results include infinite stresses at the contact line. Bertozzi & Brenner (1997) used the Hoffman–Voinov–Tanner rule that includes a cutoff length,

which is equivalent to a slip length, and the flow that it describes is equivalent to that obtained on using a slip velocity. However, they ignore both the fact that the base curvature is very large at the contact line, and the second contribution to the Laplace pressure discussed earlier. This term $(4\bar{H}^2 - 2\bar{K})$ is very significant near the contact line but localized there, and can destabilize its movement as will be shown subsequently.

2. A liquid drop on a horizontal solid surface and under air

The solutions to the fluid mechanics of spreading drops (Neogi & Miller 1982, 1983) assume that the drops have spread sufficiently to appear flat and thin and the key features are given below. The equations of motion are simplified with the quasi-static assumption and the lubrication theory assumption. Under the latter, only the velocity in the tangential (r) direction, $\bar{v}_r$ is important and varies mainly in the normal (z) direction, leading to

$$-\frac{\partial \bar{p}}{\partial r} + \mu \frac{\partial^2 \bar{v}_r}{\partial z^2} \approx 0, \tag{2.1}$$

$$-\frac{\partial \bar{p}}{\partial z} \approx 0, \tag{2.2}$$

where the overbars indicate the base quantities which are to be distinguished from the perturbations to appear soon. The coordinates are shown in figure 1. Here, μ is the viscosity and $\bar{p}$ is the pressure. If the drop height is of the order of H and the lateral dimension L, then under the lubrication theory approximation the slope of the drop profile $\sim H/L$, is small and can be ignored. This leads to the equations of motion given above, and the following boundary conditions, which are similar to those that apply to a film of constant thickness:

zero shear

$$\frac{\partial \bar{v}_r}{\partial z} = 0 \quad \text{at} \quad z = \bar{h}, \tag{2.3}$$

slip

$$\bar{v}_r = -\frac{l^2}{3\mu}\frac{\partial \bar{p}}{\partial r} \quad \text{at} \quad z = 0, \tag{2.4}$$

normal stress

$$\bar{p} = -\gamma \left[\frac{\partial^2 \bar{h}}{\partial r^2} + \frac{1}{r}\frac{\partial \bar{h}}{\partial r}\right] \quad \text{at} \quad z = \bar{h}, \tag{2.5}$$

where $\bar{h}$ is the local drop thickness and l is the slip length. The pressure, as given by the product of surface tension and the approximate form of curvature appropriate when the drop is flat in (2.5), is the same for all values of z as seen in (2.2). The order of the mean curvature here, $\sim H/L^2$, is small and the pressure gradient that it gives rise to is $\sim H/L^3$, still smaller. However, if this term is ignored, only the equilibrium situation can be described. Hence under the lubrication theory approximation, to the leading order the dynamics problem is a small-velocities problem, as seen in the expression for the spreading rate, (2.9) below. More details on the scaling under the lubrication theory approximation as applicable to the wetting kinetics problem are given by Voinov (1976).

Equation (2.1) can be integrated to obtain the velocity, which is then averaged over the local drop thickness to get

$$\langle \bar{v}_r \rangle = -\frac{1}{3\mu}\frac{\partial \bar{p}}{\partial r}(\bar{h}^2 + l^2). \tag{2.6}$$

It can be shown that the slip velocity at the contact line is equal to the average velocity at the contact line and the contact line velocity, i.e.

$$\bar{v}_r(z = 0,\ r = \bar{r}_0,\ \bar{h} = 0) = \langle \bar{v}_r \rangle (r = \bar{r}_0,\ \bar{h} = 0) = \frac{\mathrm{d}\bar{r}_0}{\mathrm{d}t}, \tag{2.7}$$

where $\bar{r}_0$ is the location of the contact line. Equation (2.6) was solved with the continuity equation to get the drop profile and the spreading rate (Neogi & Miller 1982, 1983). The latter is given in (1.1). The drop shapes were found to be spherical caps, except in the immediate vicinity of the contact line where the profile turned sharply to form a precursor film which retained a zero contact angle at the contact line. That is, the theory predicts that at the location determined under microscopy to be the contact line, the drop has a very large curvature. The solution was obtained using the method of matched asymptotic expansions based on the fact that the slip length l is a small quantity. The domain is split into the outer region which is the region where the basic shape of the drop is that of a spherical cap, the inner region of the extended thin film, and the intermediate region of very large curvature at the base of the drop.

The gauge used for constructing these solutions is ε, equal to the dimensionless slip length $l/V^{1/3}$, where V is the drop volume. To the leading order the dimensionless drop thickness is $O(1)$ in the outer and intermediate regions, and $O(\sigma^2[\ln|1/\varepsilon|]^{-1}/\varepsilon)$ in the inner region, where $\mathrm{ord}\,(\sigma^2) < \mathrm{ord}\,(\varepsilon)$. The pressure gradients and the velocities are uniformly of $O([\ln|1/\varepsilon|]^{-1})$, all expressed in outer variables. Since the gauge function here is different from those used in the lubrication theory approximation, it is worth examining the slopes in the different regions. These are $O(1)$ in the outer, $O(\varepsilon)$ in the intermediate and $O(\sigma^3[\ln|1/\varepsilon|]^{-1}/\varepsilon)$ in the inner, all expressed in outer variables. Since the thickness and lateral dimensions are non-dimensionalized with H and L respectively, the above slopes have to be multiplied by H/L to obtain the slopes in terms of the primitive variables. These are all seen to be small.

The solution from the intermediate region (Neogi & Miller 1982, 1983) can be used to show that the curvature there is

$$\frac{\mathrm{d}^2\bar{h}}{\mathrm{d}r^2} = \frac{\pi}{2\lambda_a l}\frac{3\mu}{\gamma}\frac{\mathrm{d}\bar{r}_0}{\mathrm{d}t}, \tag{2.8}$$

where

$$\frac{\mathrm{d}\bar{r}_0}{\mathrm{d}t} = \frac{\gamma}{3\mu}[\ln|1/\varepsilon|]^{-1}\left[\frac{4V}{\pi}\right]^3 \bar{r}_0^{-9}. \tag{2.9}$$

One additional result that

$$\left.\frac{\partial^2 \bar{v}_r}{\partial z^2}\right|_{z=\bar{h}} = -\frac{1}{l^2}\frac{\mathrm{d}\bar{r}_0}{\mathrm{d}t} \tag{2.10}$$

is noted for future reference. It is large because the slip length appears in the denominator on the right-hand side of (2.10). The first derivative of the velocity at the air–liquid interface is zero, and the velocity itself at this interface is smaller than the right-hand side of (2.10) by a factor of $\bar{h}^2$, which is small in the vicinity of the contact line.

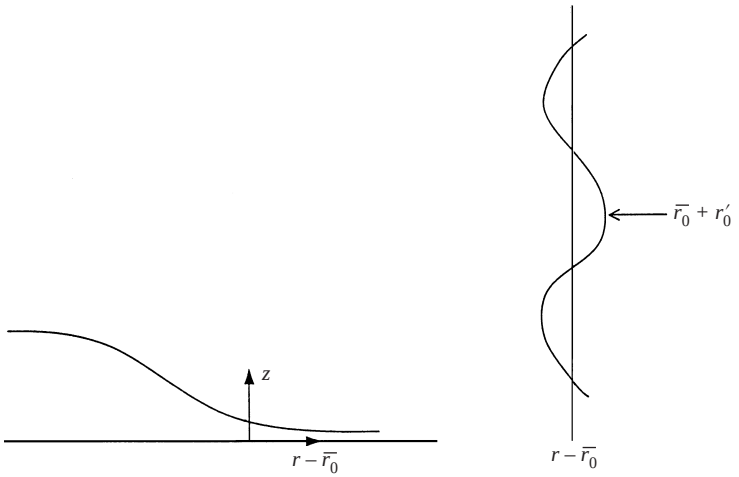

FIGURE 2. The perturbations observed at $r = \bar{r}_0$, and the transformed coordinates are shown in plan view. On the left is the bulk liquid visible under a microscope and on the right is the precursor film not observable under the microscope. The demarcating contact line is clearly visible.

Consider now that the base case receives a small perturbation. The linearized equations of motion and continuity become

$$\rho\left[\frac{\partial \boldsymbol{v}'}{\partial t} + \bar{v}_r\frac{\partial \boldsymbol{v}'}{\partial r} + v'_z\frac{\partial \bar{v}_r}{\partial z}\boldsymbol{e}_r\right] = -\nabla p' + \mu\nabla^2\boldsymbol{v}', \tag{2.11}$$

$$\nabla\cdot\boldsymbol{v}' = 0, \tag{2.12}$$

where the primes denote the small perturbation. It is assumed that the perturbations grow faster than the rate at which the basic drop spreads, and the unsteady-state term is thus retained. That is, there are two time scales in the problem: a small time scale which tracks the growth of instability and a large time scale over which the basic drop moves. The latter is approximated to be frozen under the above assumption. The convective terms are ignored under the assumption that the velocity and the velocity gradient from the base case are very small near the contact line, being dependent on $\bar{h}$. It can be further assumed that it is possible to confine the analysis to the contact line region, that is to large values of $r - \bar{r}_0$. This amounts to a shift in coordinates as shown in figure 2. For large $\bar{r}_0$, the curvature of the basic drop in the θ-direction can be ignored. The governing equations now become in cylindrical coordinates

$$\rho\frac{\partial v'_r}{\partial t} = -\frac{\partial p'}{\partial r} + \mu\left[\frac{\partial^2 v'_r}{\partial r^2} + \frac{1}{\bar{r}_0^2}\frac{\partial^2 v'_r}{\partial\theta^2} + \frac{\partial^2 v'_r}{\partial z^2}\right], \tag{2.13}$$

$$\rho\frac{\partial v'_\theta}{\partial t} = -\frac{1}{\bar{r}_0}\frac{\partial p'}{\partial\theta} + \mu\left[\frac{\partial^2 v'_\theta}{\partial r^2} + \frac{1}{\bar{r}_0^2}\frac{\partial^2 v'_\theta}{\partial\theta^2} + \frac{\partial^2 v'_\theta}{\partial z^2}\right], \tag{2.14}$$

$$\rho\frac{\partial v'_z}{\partial t} = -\frac{\partial p'}{\partial z} + \mu\left[\frac{\partial^2 v'_z}{\partial r^2} + \frac{1}{\bar{r}_0^2}\frac{\partial^2 v'_z}{\partial\theta^2} + \frac{\partial^2 v'_z}{\partial z^2}\right], \tag{2.15}$$

$$\frac{\partial v'_r}{\partial r} + \frac{1}{\bar{r}_0}\frac{\partial v'_\theta}{\partial\theta} + \frac{\partial v'_z}{\partial z} = 0. \tag{2.16}$$

The solution is sought in the form $(v'_r, v'_\theta, v'_z, p') = [u(z), v(z), w(z), \Pi(z)]\,\mathrm{e}^{\beta t}\,\mathrm{e}^{-\mathrm{i}\omega(r-\bar{r}_0)}\,\mathrm{e}^{\mathrm{i}n\theta}$, where new coordinates of figure 2 have been used. For convenience, the equation

$\nabla^2 p' = 0$ which is valid in the present case is also used:

$$\frac{\partial^2 p'}{\partial r^2} + \frac{1}{\bar{r}_0^2}\frac{\partial^2 p'}{\partial \theta^2} + \frac{\partial^2 p'}{\partial z^2} = 0. \tag{2.17}$$

Substituting this form of solution into (2.13) to (2.17) leads to

$$\rho\,\beta\,u = \mathrm{i}\omega\Pi + \mu\left[-\omega^2 - \frac{n^2}{\bar{r}_0^2} + \frac{\mathrm{d}^2}{\mathrm{d}z^2}\right]u, \tag{2.18}$$

$$\rho\,\beta\,v = -\frac{\mathrm{i}n}{\bar{r}_0}\Pi + \mu\left[-\omega^2 - \frac{n^2}{\bar{r}_0^2} + \frac{\mathrm{d}^2}{\mathrm{d}z^2}\right]v, \tag{2.19}$$

$$\rho\,\beta\,w = -\frac{\mathrm{d}\Pi}{\mathrm{d}z} + \mu\left[-\omega^2 - \frac{n^2}{\bar{r}_0^2} + \frac{\mathrm{d}^2}{\mathrm{d}z^2}\right]w, \tag{2.20}$$

$$-\mathrm{i}\,\omega\,u + \frac{\mathrm{i}n}{\bar{r}_0}v + \frac{\mathrm{d}w}{\mathrm{d}z} = 0, \tag{2.21}$$

$$\left[-\omega^2 - \frac{n^2}{\bar{r}_0^2} + \frac{\mathrm{d}^2}{\mathrm{d}z^2}\right]\Pi = 0. \tag{2.22}$$

Equation (2.22) is solved to get

$$\Pi = A\sinh(z\alpha_1) + B\cosh(z\alpha_1). \tag{2.23}$$

Substituting (2.23) into (2.18)–(2.20) leads to equations that can be solved for the velocities, leading to

$$u = C\sinh(z\alpha_2) + D\cosh(z\alpha_2) + \frac{\mathrm{i}\omega}{\rho\beta}[A\sinh(z\alpha_1) + B\cosh(z\alpha_1)], \tag{2.24}$$

$$v = E\sinh(z\alpha_2) + F\cosh(z\alpha_2) - \frac{\mathrm{i}n}{\bar{r}_0\rho\beta}[A\sinh(z\alpha_1) + B\cosh(z\alpha_1)], \tag{2.25}$$

$$w = G\sinh(z\alpha_2) + H\cosh(z\alpha_2) - \frac{\alpha_1}{\rho\beta}[A\cosh(z\alpha_1) + B\sinh(z\alpha_1)], \tag{2.26}$$

where $A, B, C, \ldots, H$, are constants of integration, and

$$\alpha_1^2 = \frac{n^2}{\bar{r}_0^2} + \omega^2, \tag{2.27}$$

$$\alpha_2^2 = \alpha_1^2 + \frac{\rho\beta}{\mu}. \tag{2.28}$$

Substituting the velocities into the continuity equation (2.21), one has

$$-C\mathrm{i}\omega + \frac{\mathrm{i}nE}{\bar{r}_0} + H\alpha_2 = 0, \tag{2.29}$$

$$-D\mathrm{i}\omega + \frac{\mathrm{i}nF}{\bar{r}_0} + G\alpha_2 = 0. \tag{2.30}$$

The boundary conditions at $z = 0$ are those of slip

$$v_r' = -\frac{l^2}{3\mu}\frac{\partial p'}{\partial r}, \tag{2.31}$$

$$v'_\theta = -\frac{l^2}{3\mu \bar{r}_0}\frac{\partial p'}{\partial \theta}, \tag{2.32}$$

and of no penetration

$$v'_z = 0. \tag{2.33}$$

The perturbed liquid–air interface is at $z = \bar{h} + \bar{h}'$, with $h' = I\mathrm{e}^{\beta t}\,\mathrm{e}^{-\mathrm{i}\omega(r-r_0)}\,\mathrm{e}^{\mathrm{i}n\theta}$, where I is a constant. Such a perturbation satisfies the constant volume requirement and forces fluctuations in the θ-direction to have only discrete wavelengths. It is not necessary to include only real values of ω which denote wave motion; imaginary values which denote spatial instabilities are also permissible. It is required that $h'/\bar{h}$ be small everywhere, because $\bar{h}$ decreases as the contact line is approached, although it does not go to zero in the region of interest, as shown in figure 1. The boundary conditions at that interface (Higgins *et al.* 1977) are simplified by using the lubrication theory approximation under which $\partial\bar{h}/\partial r$ is small, as are the perturbed quantities and all the fluid mechanical quantities in the base case which appear (with the exception of the term in (2.10)) because they are small, being dependent on $\bar{h}$. In addition the base shear stress is zero at $z = \bar{h}$. The resulting boundary conditions that are linearized about the location $z = \bar{h}$ are those of zero shear

$$\frac{\partial v'_\theta}{\partial z} + \frac{1}{\bar{r}_0}\frac{\partial v'_z}{\partial \theta} = 0, \tag{2.34}$$

$$\frac{\partial v'_z}{\partial r} + \frac{\partial v'_r}{\partial z} + \frac{\partial^2 \bar{v}_r}{\partial z^2}h' = 0, \tag{2.35}$$

kinematics

$$\frac{\partial h'}{\partial t} = v'_z, \tag{2.36}$$

and the normal stress balance

$$\frac{\partial \bar{p}}{\partial z}h' + p' - 2\mu\frac{\partial v'_z}{\partial z} = -\gamma\left[\frac{\partial^2 h'}{\partial r^2} + \frac{1}{\bar{r}_0}\frac{\partial h'}{\partial r} + \frac{1}{\bar{r}_0^2}\frac{\partial^2 h'}{\partial \theta^2}\right] + \gamma\left[\frac{\partial^2 \bar{h}}{\partial r^2}\right]^2 h'. \tag{2.37}$$

It is noteworthy that some base quantities become included in the boundary conditions when the boundary is moved from $\bar{h} + h'$ to $\bar{h}$. The second derivative of the base velocity determined earlier in (2.10) appears in (2.35). It is the largest term involving the base velocity to appear in the equations governing the perturbations, and the only one among such terms that has been retained based on magnitudes. In (2.37) the base pressure gradient is seen to be zero from (2.2). The last term in this equation is very important and arises when the base profile is curved.

Substituting the solutions into the boundary conditions, together with (2.29) and (2.30), one has a set of equations which can be expressed as a matrix equation

$$\boldsymbol{Q}\boldsymbol{q} = \boldsymbol{0}, \tag{2.38}$$

where $\boldsymbol{Q}$ is a 9×9 matrix and $\boldsymbol{q}$ is a column vector made up of constants $A, B, C, \ldots, H, I$. For these constants to have a non-trivial solution, the determinant of $\boldsymbol{Q}$ must vanish. Since the solution is confined to the region near the contact line, one additional simplification that $\bar{h}$ is very small is made, which is equivalent to the assumptions that $\alpha_1\bar{h} \ll 1$ and $\alpha_2\bar{h} \ll 1$. Expansions of functions of $\bar{h}$ are taken up to terms of the order of $\bar{h}^3$ to obtain the results given below. This assumption becomes invalid for disturbances of small wavelengths. However, the physical effect at small wavelengths is known, in that such disturbances are stable because of the effect of

surface tension which acts to reduce the very large areas that are created. When the determinant is zero, one has

$$\beta = -\mathrm{i}\omega \frac{\partial^2 \bar{v}_r}{\partial z^2}\bar{h}^2 - \frac{\alpha_1^2 \bar{h}^3}{3\mu}\gamma \left[\alpha_1^2 - \left(\frac{\mathrm{d}^2\bar{h}}{\mathrm{d}r^2}\right)^2\right], \tag{2.39}$$

where one term in the expression for curvature has been ignored under the assumption that $\bar{r}_0$ is large. It is seen that the effects of slip length are negligible at this order of approximation. In particular, (2.39) has been arrived at by assuming that l is no larger than $\bar{h}$. When the curvature is large, (2.39) becomes

$$\beta \simeq \frac{\alpha_1^2 \bar{h}^3 \gamma}{3\mu}\left(\frac{\mathrm{d}^2\bar{h}}{\mathrm{d}r^2}\right)^2, \tag{2.40}$$

that is, the system can become unstable due to large curvature near the contact line.

3. A liquid drop on a horizontal solid surface under a very viscous ambient liquid

This case is very similar to one analysed above except that the boundary condition at the drop–ambient liquid interface changes to that of no slip, that is (2.3) changes to

$$\bar{v}_r = 0 \quad \text{at} \quad z = \bar{h} \quad \text{(no-slip)}. \tag{3.1}$$

Equation (2.6) becomes

$$\langle \bar{v}_r \rangle = -\frac{1}{12\mu}\frac{\partial \bar{p}}{\partial r}(\bar{h}^2 + 6l^2). \tag{3.2}$$

Equation (2.9) changes to

$$\frac{\mathrm{d}\bar{r}_0}{\mathrm{d}t} = -\frac{l^2}{2\mu}\frac{\partial \bar{p}}{\partial r} \tag{3.3}$$

and a quantity that is needed later changes from zero to

$$\left.\frac{\partial \bar{v}_r}{\partial z}\right|_{z=\bar{h}} = \frac{1}{2\mu}\frac{\partial \bar{p}}{\partial r}\left[\bar{h} + \frac{2l^2}{3\bar{h}}\right] = -\frac{3}{2l^2}\frac{\mathrm{d}\bar{r}_0}{\mathrm{d}r}\left[\bar{h} + \frac{2l^2}{3\bar{h}}\right], \tag{3.4}$$

that is, the shear stress at the contact line becomes infinite in spite of slip at the solid–liquid interface. This is due to the fact that the no-slip condition at the liquid–liquid interface in this case is an approximation which is not always reliable. In what follows the contact line region will be assumed to have very small values of $\bar{h}$ but still larger than slip length l. The average velocity in (3.2) is the same as that in (2.6) except for some constants. Both equations are solved for drop profiles using an integral form of the continuity equation subject to initial and boundary conditions. Since these are the same for both cases, the solutions are also same, with minor changes in the constants as seen on comparing (2.6) and (3.2).

Among the perturbed quantities, the boundary conditions at $z = \bar{h}$ become

$$v_\theta' = 0, \tag{3.5}$$

$$v_r' + \frac{\partial \bar{v}_r}{\partial z}h' = 0, \tag{3.6}$$

which replace (2.34) and (2.35).

The procedure now is same as before. Equations (2.23)–(2.26) are still valid solutions

to the perturbations. One obtains a matrix equation like (2.38). The determinant of the square matrix for small values of $\bar{h}$ yields terms up to $\bar{h}^3$:

$$\beta = -\mathrm{i}\omega \frac{\partial \bar{v}_r}{\partial z} \frac{\bar{h}}{2}. \tag{3.7}$$

It appears therefore that the no-slip boundary condition at the liquid–liquid interface is too strong and freezes out the important modes of instability. This case will not be considered any further.

4. Results and discussion

Substituting into (2.39) from (2.8) and (2.10), one has

$$\beta = \mathrm{i}\omega \left[\frac{\bar{h}}{l}\right]^2 \frac{\mathrm{d}\bar{r}_0}{\mathrm{d}t} - \frac{\alpha_1^4 \bar{h}^3}{3\mu}\gamma + \frac{\alpha_1^2 \bar{h}\,\pi^2\, 3\mu}{4\,\lambda_a^2\,\gamma} \left[\frac{\bar{h}}{l}\right]^2 \left[\frac{\mathrm{d}\bar{r}_0}{\mathrm{d}t}\right]^2. \tag{4.1}$$

The second term on the right-hand side is not significant unless α_1 is very large, in which case it exerts a stabilizing influence. This is the usual effect of surface tension where disturbances of small wavelengths are rendered stable. Thus, no obvious problems due to the approximation $\alpha_1\bar{h} \ll 1$ or $\alpha_2\bar{h} \ll 1$ made earlier are observed at small wavelengths. The third term on the right-hand side represents the effect of curvature. For disturbances of intermediate wavenumbers α_1 (or wavelengths) this term will dominate and will destabilize the system. It is the first term on the right-hand side that is difficult to interpret. For $\beta = 0$, $\mathrm{i}\omega$ is real and if the effect of curvature dominates, then it is negative. Since disturbances grow *spatially* as $\exp[-\mathrm{i}\omega(r - \bar{r}_0)]$, a negative real value of $\mathrm{i}\omega$ implies that the disturbances in the vicinity of the contact line decay as they travel to the interior. Although $\mathrm{i}\omega$ does not represent waves, the inverse of it represents a length scale of the region near the contact line and the disturbances near the contact line are confined to this region. However, the magnitude of this length is not known. If the magnitudes of the first and the third terms on the right-hand side are compared with nominal values of the variables, the first term is seen to be large. That is, it will dominate β unless $\mathrm{i}\omega$ is very small. Since no activity in the radial direction is seen in the experiments, $\mathrm{i}\omega$ is set to zero. Equation (4.1) becomes

$$\beta \simeq -\frac{n^2 \bar{h}^3}{3\mu\bar{r}_0^2}\gamma \left[\frac{n^2}{\bar{r}_0^2} - \left(\frac{\delta}{l}\right)^2 \left(\frac{\mathrm{d}\bar{r}_0}{\mathrm{d}t}\right)^2\right], \tag{4.2}$$

where $\delta = 3\pi\mu/(2\lambda_a\gamma)$. The smallest allowable value of n is 1. The system is unstable for $n = 1$ to $n = n_0$ where n_0 is obtained by setting β to zero, as $n_0 = \bar{r}_0(\delta/l)(\mathrm{d}\bar{r}_0/\mathrm{d}t)$. A schematic view is shown in figure 3. The fastest growing wavelength can be found from the maximum in β with respect to n in (4.2). One has

$$\beta_{\max} = \frac{\gamma}{12\mu}\left(\frac{\delta}{l}\right)^2 \bar{h}^3 \left(\frac{\mathrm{d}\bar{r}_0}{\mathrm{d}t}\right)^4, \tag{4.3}$$

which occurs at $n_m = (\bar{r}_0/\sqrt{2})(\delta/l)(\mathrm{d}\bar{r}_0/\mathrm{d}t)$. This is the fastest growing mode which for reasonable values of the parameters ($\bar{r}_0 = 0.2\,\mathrm{cm}$, $\mathrm{d}\bar{r}_0/\mathrm{d}t = 10^{-3}\,\mathrm{cm\,s^{-1}}$ since spontaneous spreading is generally of the order of $1\,\mathrm{mm\,min^{-1}}$, Bascom, Cottington & Singleterry 1964, $\mu = 1p$, $\gamma = 27\,\mathrm{dyn\,cm^{-1}}$, $\lambda_a = 0.1$, $l = 10^{-4}\,\mathrm{cm}$ for a rough surface and $10^{-7}\,\mathrm{cm}$ for a smooth surface, based on the discussion by Neogi & Miller 1982, 1983) yields $n_m = 1.7$ for a rough surface and 1745 for a smooth surface, and

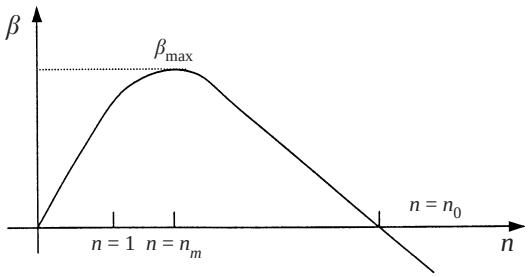

FIGURE 3. The rate of growth β plotted against n, with the key values of n shown: n_0, the marginally stable case; n_m, the fastest growing wavelength; and $n = 1$ the minimum allowable value.

the wavelengths in the θ-direction are $2\pi\bar{r}_0/n_m = 0.72\,\text{mm}$ on the rough surface and 0.00072 mm on the smooth. Both of these values appear to be reasonably within the visible range of a microscope. Since the drop volumes are of the order of $10^{-3}\,\text{cm}^3$, the dimensionless slip length ε falls in the range of 10^{-3} to 10^{-6} in these calculations. The rate of growth appears to be sensitive to the slip length with $\beta_{\max} \propto \varepsilon^{-2}[\ln|1/\varepsilon|]^{-4}$, which is also seen in the results of Bertozzi & Brenner (1997).

Since the large curvature at the contact line is so important, it is useful to reconsider the features behind it. The basic drop shape is a spherical cap with an apparent dynamic contact angle of λ_a and the profile then changes sharply to form the very thin precursor film with a contact angle of zero in accordance with the fact that it is a wetting liquid. In the case of non-wetting liquids the precursor film has to make a much less drastic turn to make a non-zero angle of $\lambda < \lambda_a$. This is much easier to achieve and the solution for the spreading drop of a non-wetting liquid shows smaller curvatures and no precursor films. No contact line instability should arise. Further, in the forced spreading encountered in most coating operations λ_a is quite large even for wetting liquids, suggesting that the curvatures at the apparent contact line are large and the contact lines are unstable, although the extent of manifestation of the instability can vary. The contact line instability is well known in forced spreading (Kistler 1993).

Although a power of 1/10 is predicted for the extent of drop spreading as a function of time (1.1), and is often observed experimentally, a power close to 1/7 is also observed for liquid drops under air (Cazabat & Cohen Stuart 1986) and under a second liquid (Lin, Neogi & Ybarra 1998). In fact even in experiments which show power of 1/10, a few runs show power of 1/7. An analysis by de Gennes (1985) equates the rate of viscous dissipation to the rate of surface work to obtain Hoffman–Voinov–Tanner rule (2.9). When the system is unstable, this balance still applies but both quantities are now different, and so the overall rate of movement is expected to be different. Thus the fact that different rates are observed at times is not surprising. Joanny & de Gennes (1984) have shown how these quantities could be calculated in the presence of waves. Those methods however require that one examines the squares of perturbed quantities, and as only linear terms have been retained here, the present results will not be useful.

To locate the contact line at $\bar{r}_0 + r_0'$, as shown in figure 2, one has

$$(\bar{h} + h')|_{r=\bar{r}_0+r_0'} \approx \bar{h}|_{r=\bar{r}_0} + \frac{\partial \bar{h}}{\partial r}|_{r=\bar{r}_0} r_0' + h'|_{r=\bar{r}_0} = 0$$

where the right-hand side becomes

$$0 + (-\lambda_a) r_0' + I\, \mathrm{e}^{\mathrm{i}n\theta}\, \mathrm{e}^{\beta t} = 0, \quad r_0' = \frac{I}{\lambda_a}\, \mathrm{e}^{\mathrm{i}n\theta}\, \mathrm{e}^{\beta t}. \tag{4.4}$$

Some of the terms that arise in (4.4) such as the amplitude of the waves (I/λ_a) and their rate of growth β, can be measured to test these results, though as yet have not been reported for a wetting liquid; however a very interesting experimental work on a perturbation about equilibrium has been reported for a non-wetting system (Ondarcuhu & Veyssie 1991). Equilibrium does not exist in a wetting system considered here. Equation (2.9) shows that the basic spreading rate has only an inverse logarithmic dependence on ε, a dependence that is too weak to evaluate ε from the experimental data with precision. However, the characteristics of the instability, being much stronger functions of ε, could provide a better way of estimating the slip length from experiments.

Consequently, the contact line instability due to the curvature effect as predicted here not only explains the existing experimental results, but it also paves the way for more focused future work, both experimental and theoretical.

The author acknowledges the many insightful comments from an unknown referee which have transformed this work much beyond its original scope.

REFERENCES

Bascom, W. D., Cottington, R. L. & Singleterry, C. R. 1964 Dynamic surface phenomena in spontaneous spreading of oils and solids. In *Contact Angle Wettability and Adhesion* (ed. R. F. Gould), p. 335. Advances in Chemistry Series, vol. 43. Am. Chem. Soc., Washington, DC.

Bertozzi, A. L. & Brenner, M. P. 1997 Linear stability and transient growth in driven contact lines. *Phys. Fluids* **9**, 530.

Cazabat, A. M. & Cohen Stuart, M. A. 1986 Dynamics of wetting: effects of roughness. *J. Phys. Chem.* **90**, 5845.

Fournier, J. B. & Cazabat, A. M. 1992 Tears of wine. *Europhys. Lett.* **20**, 517.

Gennes, P. G. de 1985 Wetting: statics and dynamics. *Rev. Mod. Phys.* **57**, 827.

Higgins, B. G., Silliman, W. J., Brown, R. A. & Scriven, L. E. 1977 Theory of meniscus shape in film flows. A synthesis. *IEC Fundam.* **16**, 393.

Huh, C. 1969 Capillary hydrodynamics: interfacial instability and the solid/liquid/fluid contact line. PhD thesis, Department of Chemical Engineering, University of Minnesota, Minneapolis.

Joanny, J.-F. & Andelman, D. 1987 Steady-state motion of a liquid/liquid/solid contact line. *J. Colloid Interface Sci.* **119**, 451.

Joanny, J.-F. & Gennes, P. G. de 1984. A model for contact line hysteresis. *J. Chem. Phys.* **81**, 552.

Kistler, S. 1993 Hydrodynamics of wetting. In *Wettability* (ed. J. C. Berg), p. 311. Marcel Dekker, Inc.

Léger, L., Erman, M., Guinet-Picart, A. M., Ausserre, D., Strazielle, C., Benattar, J. J., Rieutord, F., Daillant, J. & Bosio, L. 1988 Spreading of nonvolatile liquids on smooth solid surfaces: role of long range forces. *Rev. Phys. Appl.* **23**, 1047.

Lin, C.-M., Neogi, P. & Ybarra, R. M. 1998 Wetting kinetics of a drop on a horizontal solid surface under a viscous ambient liquid. *I & EC Res.* **37**, 66.

Lin, C.-M., Ybarra, R. M. & Neogi, P. 1996 Three- and two-dimensional effects in wetting kinetics. *Adv. Colloid Interface Sci.* **67**, 185.

Lopez, P. G., Miksis, M. J. & Bankoff, S. G. 1997 Inertial effects of contact line instability in the coating of a dry inclined plate. *Phys. Fluids* **9**, 2177.

Miller, C. A. 1978 Stability of interfaces. In *Surface and Colloid Science*, vol. 10 (ed. E. Matijevic), p. 227. Plenum.

Neogi, P. & Adib, F. 1985 Dynamic contact lines in rotating liquids. *Langmuir* **1**, 747.

Neogi, P. & Miller, C. A. 1982 Spreading kinetics of a drop on a smooth solid surface. *J. Colloid Interface Sci.* **86**, 525.

Neogi, P. & Miller, C. A. 1983 Spreading kinetics of a drop on a rough solid surface. *J. Colloid Interface Sci.* **92**, 338.

Nieh, S.-Y., Ybarra, R. M. & Neogi, P. 1996 Wetting kinetics of polymer solutions: experimental observations. *Macromolecules* **29**, 320.

Ondarcuhu, T. & Veyssie, M. 1991 Relaxation modes of the contact line of a liquid spreading on a surface. *Nature* **352**, 418.

Pitts, E. 1974 The stability of pendant liquid drops. 2. Axial symmetry. *J. Fluid Mech.* **63**, 487.

Ruckenstein, E. & Jain, R. K. 1974 Spontaneous rupture of a thin liquid film. *J. Chem. Soc. Faraday Trans. II* **70**, 132.

Troian, S. M., Herzbolzheimer, E. & Safran, S. A. 1990 Model for fingering instability of spreading surfactant drops. *Phys. Rev. Lett*. **65**, 333.

Tyupstov, A. D. 1966 Hydrostatics in weak force fields. *Fluid Dyn.* **1**, 51.

Voinov, O. V. 1976 Hydrodynamics of wetting. *Fluid Dyn.* **11**, 714.

Williams, R. 1977 The advancing front of a spreading liquid. *Nature* **266**, 153.

Ybarra, R. M., Neogi, P. & MacElroy, J. M. D. 1998 Osmotic stresses and wetting by polymer solutions. *I & EC Res.* **37**, 427.